Quantum stochastic resonance in an a.c.-driven single-electron quantum dot

Timo Wagner, Peter Talkner, Johannes C. Bayer, Eddy P. Rugeramigabo, Peter Hänggi, Rolf J. Haug

Angaben zur Veröffentlichung / Publication details:

Wagner, Timo, Peter Talkner, Johannes C. Bayer, Eddy P. Rugeramigabo, Peter Hänggi, and Rolf J. Haug. 2019. "Quantum stochastic resonance in an a.c.-driven single-electron quantum dot." *Nature Physics* 5: 330–34. https://doi.org/10.1038/s41567-018-0412-5.

Quantum stochastic resonance in an a.c.-driven single-electron quantum dot

Timo Wagner[1*], Peter Talkner[2], Johannes C. Bayer[1], Eddy P. Rugeramigabo[1], Peter Hänggi[2,3] and Rolf J. Haug[1]

In stochastic resonance, the combination of a weak signal with noise leads to its amplification and optimization[1]. This phenomenon has been observed in several systems in contexts ranging from palaeoclimatology, biology, medicine, sociology and economics to physics[1–9]. In all these cases, the systems were either operating in the presence of thermal noise or were exposed to external classical noise sources. For quantum-mechanical systems, it has been theoretically predicted that intrinsic fluctuations lead to stochastic resonance as well, a phenomenon referred to as quantum stochastic resonance[1,10,11], but this has not been reported experimentally so far. Here we demonstrate tunnelling-controlled quantum stochastic resonance in the a.c.-driven charging and discharging of single electrons on a quantum dot. By analysing the counting statistics[12–16], we demonstrate that synchronization between the sequential tunnelling processes and a periodic driving signal passes through an optimum, irrespective of whether the external frequency or the internal tunnel coupling is tuned.

Stochastic resonance is known to arise in noisy bistable systems with proper periodic modulation of the switching rates. It manifests itself as an optimal synchronization of the driving signal with the switching process, as a function of the driving frequency f as well as the noise level. As a rule of thumb, this optimum occurs at[1,13]

$$2f \approx \Gamma_{\mathrm{S}} \tag{1}$$

when the doubled driving frequency $2f$ approximately corresponds to the unperturbed switching rate Γ_{S}. The switching rate Γ_{S} thereby characterizes the noise spectrum of the system. Because stochastic resonance does not depend on the concrete physical realization of the system, this timescale matching condition should also be applicable to the tunnelling process between two quantum states. The noise source in that case is the intrinsic shot noise, which stems directly from the random quantum mechanical tunnelling dynamics. To observe stochastic resonance in an a.c.-driven quantum dot, one needs to precisely control the tunnelling process between two quantum states of the quantum dot and measure the temporal fluctuations.

Figure 1a presents a scanning electron microscopy (SEM) image of our device structure as well as a schematic of the experimental set-up. The quantum dot (green e^- island) is formed electrostatically by nanosized gate electrodes and behaves physically like an artificial atom, which can be charged or discharged via two tunnel-coupled electron reservoirs[17]. This single-electron charging process is sensed directly with the capacitively coupled quantum point contact (QPC), operated as a time-resolved charge detector[15,16]. The number N_e of bound electrons on the quantum dot is set in a controlled manner via the three gate voltages $\mathbf{V}_{\mathrm{G}} = (V_{\mathrm{d1}}, V_{\mathrm{d2}}, V_{\mathrm{d3}})$. Figure 1b presents a gate-dependent charge stability diagram of the quantum dot in the few-electron regime. Along the visible charging lines, a quantum dot charge state μ_{N} is energetically close to the Fermi level μ_{F} of the tunnel-coupled reservoirs, allowing electrons to tunnel back and forth between the quantum dot and the reservoirs. The thermal energy $k_{\mathrm{B}}T = 130\,\mu\mathrm{eV}$ at $T = 1.5\,K$ is much smaller than the charging energy $E_{\mathrm{c}} \approx 2.5\,\mathrm{meV}$. E_{c} is the difference between the electrochemical potential of the Nth and $(N-1)$st electron. Therefore, only one additional electron can occupy the quantum dot at any given time (Coulomb blockade), causing sequential 'in' and 'out' tunnelling.

We set our experimental operation point $\mathbf{V}_{\mathrm{OP}}$ at the first charging line, indicated as $N_e = 1$ in Fig. 1b, where the electron number on the quantum dot fluctuates between zero and one. For the driving we periodically modulated the three gate voltages

$$\mathbf{V}_{\mathrm{G}}(t) = \mathbf{V}_{\mathrm{OP}} + \mathbf{e}_{\mathrm{d}} A \ \sin(2\pi f t) \tag{2}$$

with frequency f, amplitude A and in the direction of the unit vector $\mathbf{e}_{\mathrm{d}}$.

To study the synchronization between the deterministic external a.c. drive and internal stochastic tunnelling process, the detector current $I_{\mathrm{qpc}}(t)$ was monitored. A short snapshot of a typical detector trace is displayed in Fig. 1c, which directly reveals the sequential charging and discharging of the quantum dot. Whenever an electron tunnels into the quantum dot the current I_{qpc} jumps down, and it jumps up again when the electron tunnels out. From the detector traces we extract the times $t_{\mathrm{in,out}}$ of all 'in' and 'out' tunnelling events (Fig. 1d).

The fluctuations in the occupation are characterized by the single-electron counting statistics[14]. We thus counted the total number $n(T_f)$ of 'in' and 'out' tunnelling events within one driving period T_f. From all possible periods and phases of the a.c. drive we finally obtained a counting probability $P(n)$ (Fig. 1e). A quantitative measure for the fluctuations is given by the Fano factor

$$F = \frac{\sigma^2}{\langle n \rangle} = \frac{\langle n^2 \rangle - \langle n \rangle^2}{\langle n \rangle} \tag{3}$$

calculated from the variance $\sigma^2 = \langle n^2 \rangle - \langle n \rangle^2$ and the mean $\langle n \rangle$ of the counting probability $P(n)$. For a strictly Poissonian random process the Fano factor equals $F = 1$. Without external a.c. drive the Fano factor always exceeds or equals this Poissonian limit (that is, $F \geq 1$) due to the bunching of tunnelling-in and tunnelling-out

[1]Institut für Festkörperphysik, Leibniz Universität Hannover, Hanover, Germany. [2]Institut für Physik, Universität Augsburg, Augsburg, Germany. [3]Nanosystems Initiative Munich, Munich, Germany. *e-mail: wagner@nano.uni-hannover.de

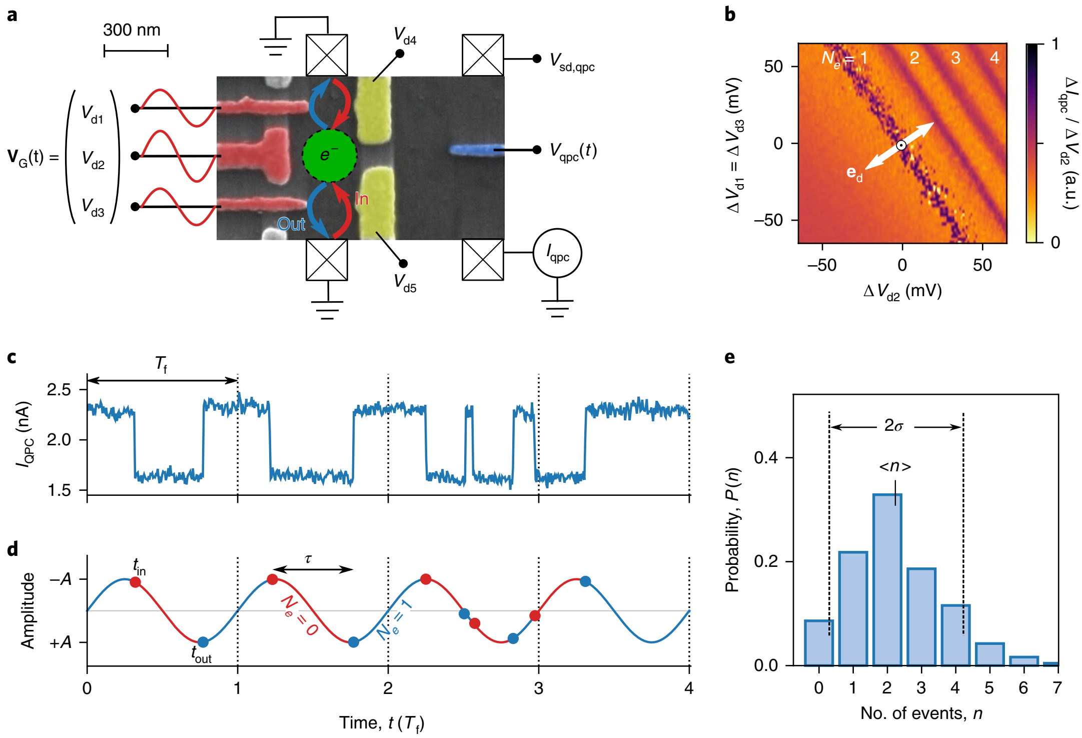

Fig. 1 | Experimental set-up, device operation and statistical analysis. a, SEM image of the device structure with a schematic of the experimental set-up. The quantum dot (green e^- island) is defined electrostatically by the red gates $V_{d1,d2,d3}$ and yellow gates $V_{d4,d5}$. The QPC charge detector is formed by the blue gate V_{qpc}. The quantum dot and QPC current paths are galvanically isolated from each other; the visible gap between the yellow middle gates is closed electrostatically and has the purpose of enhancing detector sensitivity. The quantum dot can be charged and discharged by electrons tunnelling in from (red arrow) and tunnelling out to (blue arrow) the coupled electron reservoirs. The tunnelling process is controlled and driven periodically by the three gate voltages $\mathbf{V}_G = (V_{d1}, V_{d2}, V_{d3})$. Crossed squares indicate the ohmic contacts of the sample. **b**, Charge stability diagram of the quantum dot in the few-electron regime. The operation point $\mathbf{V}_{G,OP}$ is indicated by a circle with a dot at the charging line $N_e = 1$. The gate voltages $\mathbf{V}_G$ are periodically modulated along the highlighted direction $\mathbf{e}_d$. **c**, A typical time-resolved current trace $I_{qpc}(t)$ of the QPC charge detector, revealing the sequential charging and discharging of the quantum dot. The shown trace was recorded with a drive of $f = 800$ Hz and an amplitude of $A = 10$ mV. **d**, Extracted 'in' (red) and 'out' (blue) tunnelling events relative to the external a.c. drive. The times t_{in},t_{out} and the residence times τ are extracted from the detected events. **e**, Counting statistics $P(n)$ for the number of tunnelling events within one driving period T_f. The Fano factor $F = \sigma^2/\langle n\rangle$, equation (3), of the distribution is calculated from the mean $\langle n\rangle$ and variance $\sigma^2 = \langle n^2\rangle - \langle n\rangle^2$ of the distribution.

events (Supplementary Fig. 1). The driving-dependent antibunching of tunnelling events, signalled by a suppression of the Fano factor below the Poissonian limit (that is, $F < 1$) thus provides an unambiguous measure of the synchronization strength[14].

The red circles in Fig. 2 depict the experimentally determined Fano factor F as a function of external driving frequency f. Additionally, the inset shows the corresponding mean counts $\langle n\rangle$ per period. The amplitude $A = 10$ mV was kept constant for all frequencies. The experimental Fano factor F has a minimum at $f = 800$ Hz, providing evidence for stochastic resonance. At the minimum, essentially two tunnelling events (one 'in' and one 'out') occur on average per driving period ($\langle n\rangle \approx 2$), corroborating the optimal synchronization between external a.c. drive and internal tunnelling. If the a.c. drive is too slow ($f \ll 800$ Hz), more than two tunnelling events occur within one period ($\langle n\rangle \gg 2$) and the Fano factor F increases above the Poissonian limit. If the drive is instead too fast ($f \gg 800$ Hz), most electrons need multiple periods to tunnel in and out of the quantum dot ($\langle n\rangle \ll 2$) and the Fano factor F approaches the Poissonian limit from below.

Because the 'in' and the 'out' tunnelling events are alternating, and hence their occurrences are strictly dependent, stochastic resonance can be equally characterized on the basis of the occurrences of the specific tunnel events (Supplementary Fig. 2) or on the basis of the set of all transitions independent of their direction, as we do here. To demonstrate, in the presently investigated system, that the general mechanisms of stochastic resonance are at play, we extracted the tunnelling rates $\Gamma_{in}(t)$ and $\Gamma_{out}(t)$ with which an electron enters and leaves the quantum dot at time t, respectively, from the experimental data (see Methods).

Figure 3a displays the tunnelling-in and tunnelling-out rates for a quantum dot with driving frequency $f = 800$ Hz and amplitude $A = 10$ mV in the direction $\mathbf{e}_d$, as indicated in Fig. 1b. The in rate (red) instantly follows the external a.c. driving voltage, as given by equation (2), without any visible delay, corroborated by the fact that the rate at half of the period agrees with its initial value, $\Gamma_{in}(0) = \Gamma_{in}(T_f/2)$. The out rate (blue) is shifted by a half period $T_f/2$ relative to the in rate and also agrees at half of the period with its initial value, $\Gamma_{out}(0) = \Gamma_{out}(T_f/2)$. This asymmetric modulation of the rates is caused by the periodic shift of the charging state $\mu_0(t)$ around the symmetry level μ_S, as illustrated in Fig. 3b. At the symmetry level $\mu_S = \mu_0\left(t = 0, \frac{1}{2}T_f, T_f, \ldots\right)$ the in and out rates are equal. In the first half of a period ($0 < t < T_f/2$) the charging state is pushed below the symmetry level, that is $\mu_0 < \mu_S$, causing an enhancement of the in rate and a suppression of the out rate. An electron tunnels from the reservoir most probably into the quantum dot when the charge state is at its energetically lowest position $\left(t = \frac{1}{4}T_f, \frac{5}{4}T_f, \ldots\right)$. In the second half of a period ($T_f/2 < t < T_f$) the charging state is instead pushed above the symmetry level,

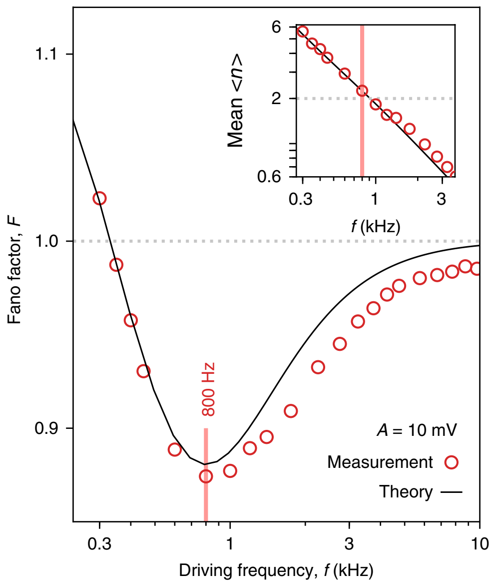

Fig. 2 | Frequency-dependent stochastic resonance. Experimental (red circles) and theoretical (black line) Fano factor F as a function of driving frequency f. The experimental data have a minimum at $f = 800$ Hz, in good agreement with the theoretical resonance frequency. Inset, Corresponding average number of tunnelling events per period $\langle n \rangle$. At the resonance frequency (vertical red line) nearly two tunnelling events ($\langle n \rangle \approx 2$) occur on average per period.

that is $\mu_0 > \mu_S$. There, the in rate is suppressed and the out rate is enhanced. The best opportunity to tunnel out occurs at the energetically highest position $\left(t = \frac{3}{4}T_f, \frac{7}{4}T_f, \ldots\right)$. The transition rates $\Gamma_{in}(t)$ and $\Gamma_{out}(t)$ specify a two-state Markovian process for which the counting probability $P(n)$ can be determined[13,14] (see Methods). The theoretical results for the first moment of the number of transitions and the Fano factor are in good agreement with the respective direct experimental outcomes, as can be seen from Figs. 2 and 4.

The resonance frequency $f = 800$ Hz at which the Fano factor attains its minimum also conforms well with the stochastic rule of thumb. The double resonance frequency $2f \approx 1{,}600$ Hz approximately matches the tunnel coupling $\Gamma_s \approx 1{,}675$ Hz at the symmetry level μ_S. When the driving frequency is much faster than the tunnel coupling (that is, $\Gamma_s \ll 2f$, an electron easily 'misses' the first good opportunity to tunnel and will wait until another good opportunity occurs, one or several periods later. These findings show that the variation of the frequency f conforms well with the idea of stochastic resonance as a resonance phenomenon.

The so-called 'residence time' is given by the time span during which a quantum dot is occupied without interruption[1]. As a random variable it is characterized by a probability density function (p.d.f.), denoted as $\rho_1(\tau)$. The blue dots in Fig. 3c display the experimentally determined residence time p.d.f. The residence time p.d.f. for fast driving with $f = 10$ kHz consists of a train of maxima at odd integer multiples of the half period[1], that is $\tau_k = (2k+1)T_f/2$, $k = 0,1,2,\ldots$, demonstrating the waiting of the electron for a good tunnelling opportunity. At the resonance frequency $f = 800$ Hz instead, obeying $2f \approx \Gamma_S$, $\rho_1(\tau)$ quickly decreases with increasing residence times with a strong shoulder at $T_f/2$ and a weak shoulder at $3T_f/2$, indicating optimal synchronization between internal tunnelling and the external a.c. drive.

Under the assumption that the time-periodic rates $\Gamma_{in/out}(t)$ govern a Markovian process of alternate visits of the occupied (1) and empty (0) quantum dot states, the residence time p.d.f., $\rho_1(\tau)$, can be calculated[14] (see Methods). Figure 3c demonstrates that the residence time p.d.f.s from the Markovian model (solid lines) agree nicely with experimental statistics.

So far, we have succeeded in showing that the synchronization can be optimized by tuning the driving frequency f. Alternatively, one may aim at synchronizing a signal at fixed frequency f. Thereby, the tunnel coupling Γ_S needs to be adapted to the double driving frequency $2f$. The coupling Γ_S depends on the size of the tunnel barriers, as illustrated in Fig. 4a. We tuned the coupling by shifting the operation point $\mathbf{V}_{G,OP}$ along the charging line (Fig. 1b). The driving frequency $f = 1$ kHz and the amplitude $A = 10$ mV were kept constant. The experimentally determined Fano factor F is plotted as a function of the tunnel coupling Γ_S in Fig. 4b and the inset shows the corresponding mean $\langle n \rangle$ of the counting statistics. The experimental Fano factor F has a minimum at 1.75 kHz, which is close to the double driving frequency $2f = 2$ kHz. At the minimum we also find nearly two tunnelling events per period

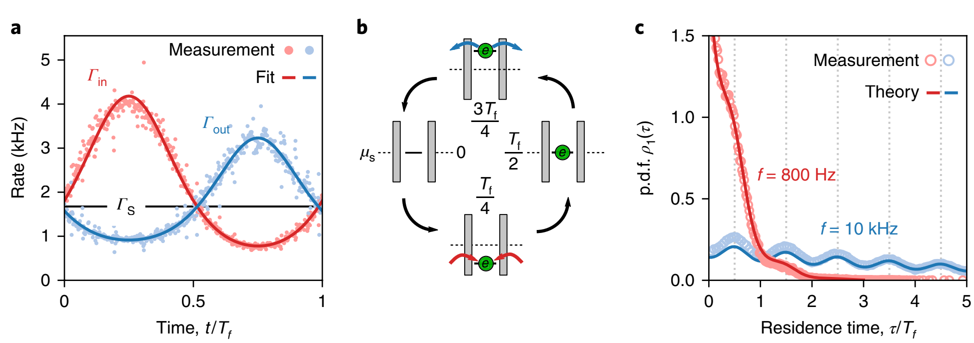

Fig. 3 | Temporal modulation of the tunnelling process. a, Experimentally time-dependent tunnelling-in rate $\Gamma_{in}(t)$ (red dots) and tunnelling-out rate $\Gamma_{out}(t)$ (blue dots). The rates were extracted for a drive with $f = 800$ Hz and $A = 10$ mV. The fits (solid lines) are based on a Fourier expansion of the logarithm of the rates. The horizontal black line marks the tunnel coupling $\Gamma_S = 1{,}675$ Hz at symmetry level μ_S. **b**, Asymmetric modulation of the rates is caused by the periodic shift of the quantum dot charging state around the symmetry level μ_S. At the symmetry level μ_S ($t = 0$, $T_f/2$), the two tunnelling rates are identical. An electron tunnels from reservoirs most probably into the quantum dot when the charge state is at its lowest position ($t = T_f/4$). The best opportunity to tunnel out of the quantum dot occurs when the charging state reaches its energetically highest position ($t = 3T_f/4$). **c**, Periodic modulation of the tunnelling process is also observable in the residence time probability density $\rho_1(\tau)$. For a fast driving frequency $f = 10$ kHz, the residence time probability density function (p.d.f.) $\rho_1(\Delta t)$ displays a train of maxima at odd integer multiples of the half period $\tau_k = (2k+1)T_f/2$, $k = 0,1,2,\ldots$ At the lower driving frequency $f = 800$ Hz, the maximum at $T_f/2$ is accompanied by considerably suppressed satellites. In both cases the agreement between experiment (dots) and theory (solid lines) is striking.

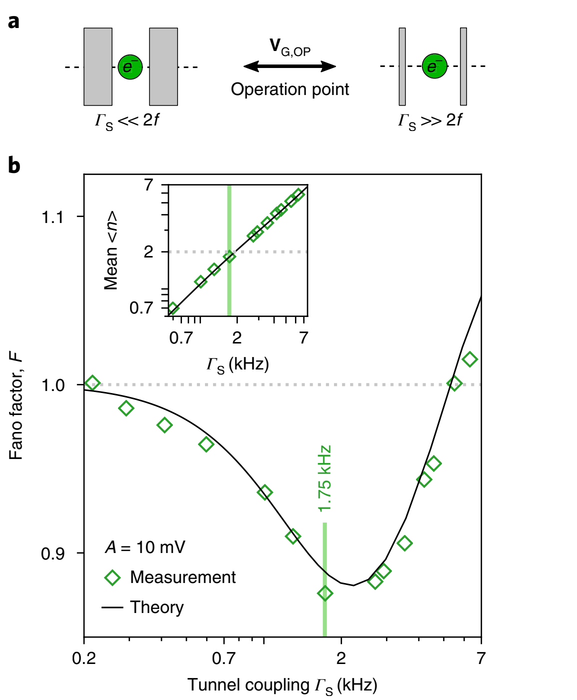

Fig. 4 | Tunnel coupling-dependent stochastic resonance. a, The tunnel coupling Γ_S of the quantum dot depends on the size of the tunnel barriers, which can be altered by choosing a different operation point $V_{G,OP}$ on the first charging line. This way, the tunnel coupling can be tuned from values smaller than to values much larger than the double driving frequency $2f$. **b**, Experimental (green diamonds) and theoretical (black line) Fano factor F as a function of tunnel coupling Γ_S. The experimental data have a minimum at $\Gamma_S = 1.75$ kHz, in good agreement with the minimum of the theoretical model. The driving parameters were $f = 1$ kHz and $A = 10$ mV. Inset, Corresponding average number of tunnelling events per period $\langle n \rangle$ as a function of tunnel coupling. At the resonance frequency (vertical green line) nearly two tunnelling events (for example, $\langle n \rangle \approx 2$; one 'in' and one 'out') occur on average per period.

($\langle n \rangle \approx 2$), corroborating the optimal synchronization of the Rice frequency defined as the rate of transition events into the occupied state[12,13]. Furthermore, we compared the experimental results with the outcome of the Markovian two-state model. According to our empirical finding the rates at different operation points are proportional to the tunnel coupling Γ_S. Therefore, the rates are given by $\Gamma_{in/out}(t, \Gamma_S) = (\Gamma_S/\Gamma_S^*)\Gamma_{in/out}(t, \Gamma_S^*)$. As reference we chose the extracted tunnelling rates (see Methods) with $\Gamma_S^* = 1{,}675$ Hz. Figure 4 displays good agreement between the resulting theoretical Fano-factors and the average numbers of transitions with the according experimental findings.

We emphasize that there is a crucial difference between the variation of the external driving frequency f and the internal tunnel coupling Γ_S. With a change of frequency f, the time averages of the transition rates as well as the values of their minima and maxima remain the same, while both rate characteristics alter upon a variation of the tunnel coupling Γ_S. Hence the variation of Γ_S corresponds more closely to the original characterization of the stochastic resonance phenomena, indicating that an increase of the noise up to a certain level can lead, counter-intuitively, to an improved signal-to-noise ratio.

Such a.c.-driven single-electron tunnelling has also been studied intensively in the form of turnstiles[18], ratchets[19] and pumps[20], the latter being promising candidates for the redefinition of the ampere[21]. The functionality of these devices is based on the locking of the mean counts $\langle n \rangle =$ const., meaning that the number of transferred electrons per period is frequency independent and robust against noise. For the stochastic resonance discussed here with a relatively weak driving amplitude $A = 10$ mV, locking is not present, as is evident from the inset of Fig. 2. The observed synchronization is a consequence of the timescale matching of the external a.c. drive and the internal tunnelling process. At a larger amplitude, $A = 30$ mV (Supplementary Fig. 3), however, the average number of transitions starts to develop plateaux around the respective resonance values of frequency and tunnel coefficient, in accordance with theoretical[12–14] and experimental[22] observations for strongly a.c.-driven stochastic resonance systems. This confirms that the locking in a.c.-driven single-electron devices is subject to the same statistical physics and can be seen as a special case of stochastic resonance in the limit of strong a.c. driving.

Stochastic resonance in a.c.-driven single-electron tunnelling should also occur in direct shot-noise measurements[23] or corresponding heat and work distributions[24]. The optimal working point for on-demand single-electron sources[25,26], which provide an important toolbox for quantum electronics, is defined by tunnelling-driven stochastic resonance. Quantum dots have been utilized successfully as displacement sensors for nanomechanical oscillators[27,28]. Their resolution is thought to be limited by the standard quantum limit, due to the stochastic backaction of the single-electron tunnelling process. The phenomenon of tunnelling-driven stochastic resonance provides a way to overcome this limit.

Online content

Any methods, additional references, Nature Research reporting summaries, source data, statements of data availability and associated accession codes are available at https://doi.org/10.1038/s41567-018-0412-5.

References

1. Gammaitoni, L., Hänggi, P., Jung, P. & Marchesoni, F. Stochastic resonance. *Rev. Mod. Phys.* **70**, 223–288 (1998).
2. Lee, I. Y., Liu, X. L., Kosko, B. & Zhou, C. W. Nanosignal processing: stochastic resonance in carbon nanotubes that detect subthreshold signals. *Nano Lett.* **3**, 1683–1686 (2003).
3. Badzey, R. L. & Mohanty, P. Coherent signal amplification in bistable nanomechanical oscillators by stochastic resonance. *Nature* **437**, 995–998 (2005).
4. Nishiguchi, K. & Fujiwara, A. Detecting signals buried in noise via nanowire transistors using stochastic resonance. *Appl. Phys. Lett.* **101**, 193108 (2012).
5. Venstra, W. J., Westra, H. J. R. & van der Zant, H. S. J. Stochastic switching of cantilever motion. *Nat. Commun.* **4**, 2624 (2013).
6. Abbaspour, H., Trebaol, S., Morier-Genoud, F., Portella-Oberli, M. T. & Deveaud, B. Stochastic resonance in collective exciton–polariton excitations inside a GaAs microcavity. *Phys. Rev. Lett.* **113**, 057401 (2014).
7. Sun, G. et al. Detection of small single-cycle signals by stochastic resonance using a bistable superconducting quantum interference devices. *Appl. Phys. Lett.* **106**, 172602 (2015).
8. Stroescu, I., Hume, D. B. & Oberthaler, M. K. Dissipative double-well potential for cold atoms: kramers rate and stochastic resonance. *Phys. Rev. Lett.* **117**, 243005 (2016).
9. Monifi, F. et al. Optomechanically induced stochastic resonance and chaos transfer between optical fields. *Nat. Photon.* **10**, 399–405 (2016).
10. Löfstedt, R. & Coppersmith, S. N. Quantum stochastic resonance. *Phys. Rev. Lett.* **72**, 1947–1950 (1994).
11. Grifoni, M. & Hänggi, P. Coherent and incoherent quantum stochastic resonance. *Phys. Rev. Lett.* **76**, 1611–1614 (1996).
12. Callenbach, L., Hänggi, P., Linz, S. J., Freund, J. A. & Schimansky-Geier, L. Oscillatory systems driven by noise: frequency and phase synchronization. *Phys. Rev. E* **65**, 051110 (2002).
13. Talkner, P. Statistics of entrance times. *Physica A* **325**, 124–135 (2003).
14. Talkner, P., Machura, Ł., Schindler, M., Hänggi, P. & Łuczka, J. Statistics of transition times, phase diffusion and synchronization in periodically driven bistable systems. *New J. Phys.* **7**, 14 (2005).
15. Gustavsson, S. et al. Counting statistics of single-electron transport in a quantum dot. *Phys. Rev. Lett.* **96**, 076605 (2006).

16. Wagner, T. et al. Strong suppression of shot noise in a feedback-controlled single-electron transistor. *Nat. Nanotechnol.* **12**, 218–222 (2017).
17. Kouwenhoven, L. P., Austing, D. G. & Tarucha, S. Few-electron quantum dots. *Rep. Prog. Phys.* **64**, 701–736 (2001).
18. Kouwenhoven, L. P., Johnson, A. T., van der Vaart, N. C., Harmans, C. J. P. M. & Foxon, C. T. Quantized current in a quantum-dot turnstile using oscillating tunnel barriers. *Phys. Rev. Lett.* **67**, 1626–1629 (1991).
19. Platonov, S. et al. Lissajous rocking ratchet: realization in a semiconductor quantum dot. *Phys. Rev. Lett.* **115**, 106801 (2015).
20. Blumenthal, M. D. et al. Gigahertz quantized charge pumping. *Nat. Phys.* **3**, 343–347 (2007).
21. Pekola, J. P. et al. Single-electron current sources: toward a refined definition of the ampere. *Rev. Mod. Phys.* **85**, 1421–1472 (2013).
22. Shulgin, B., Neiman, A. & Anishchenko, V. Mean switching frequency locking in stochastic bistable systems driven by a periodic force. *Phys. Rev. Lett.* **75**, 4157–4160 (1995).
23. Burk, H., de Jong, M. J. M. & Schönberger, C. Shot-noise in the single-electron regime. *Phys. Rev. Lett.* **75**, 1610–1613 (1995).
24. Pekola, J. P. Towards quantum thermodynamics in electronic circuits. *Nat. Phys.* **11**, 118–123 (2015).
25. Féve, G. et al. An on-demand coherent single-electron source. *Science* **316**, 1169–1172 (2007).
26. Albert, M., Flindt, C. & Büttiker, M. Distributions of waiting times of dynamic single-electron emitters. *Phys. Rev. Lett.* **107**, 086805 (2011).
27. Mozyrsky, D., Martin, I. & Hastings, M. B. Quantum-limited sensitivity of single-electron-transistor-based displacement detectors. *Phys. Rev. Lett.* **92**, 018303 (2004).
28. LaHaye, M. D., Buu, O., Camarota, B. & Schwab, K. C. Approaching the quantum limit of a nanomechanical resonator. *Science* **304**, 74–77 (2004).

Acknowledgements
This work was supported financially by the Research Training Group 1991 (DFG), the School for Contacts in Nanosystems (NTH), the Center for Quantum Engineering and Space-Time Research (QUEST), the Laboratory for Nano and Quantum Engineering (LNQE) and the 'Fundamentals of Physics and Metrology' initiative (T.W, J.C.B., E.R. and R.J.H.).

Author contributions
T.W. carried out the experiments, analysed the data and wrote the manuscript. J.C.B. and T.W. fabricated the device. E.P.R. grew the wafer material. P.T. and P.H. provided theory support. T.W., P.T., P.H. and R.J.H discussed the results. R.J.H. supervised the research. All authors contributed to editing the manuscript.

Competing interests
The authors declare no competing interests.

Additional information
Supplementary information is available for this paper at https://doi.org/10.1038/s41567-018-0412-5.

Correspondence and requests for materials should be addressed to T.W.

Methods

Experimental set-up. Our quantum dot device is based on a GaAs/AlGaAs heterostructure, which forms a two-dimensional electron gas (2DEG) 100 nm below the surface. The 2DEG charge carrier density is $n_e = 2.4\times10^{-11}$ cm, and the mobility is $\mu_e = 5.1\times10^5\,\mathrm{cm^2\,V^{-1}\,s^{-1}}$. On the surface we patterned nanosized metallic top gates (7 nm Cr, 30 nm Au) using electron-beam and optical lithography. The quantum dot and QPC are formed electrostatically. By applying negative voltages to the gates, we deplete the 2DEG below.

All measurements were carried out on a low-noise d.c. transport set-up in a ^{4}He cryostat at 1.5 K. Filtering and signal amplification were fully carried out outside the cryostat at room temperature. All gates were filtered by a 1 MHz low-pass filter. The QPC source was filtered by a 10 Hz low-pass filter and a 1:1,000 voltage divider was used to increase the resolution. The QPC charge detector current was amplified with a low-noise FEMTO transimpedance amplifier (100 MV A^{-1} gain, 100 kHz bandwidth), connected to the QPC drain by a 25 pF low-capacity coaxial line. An Adwin Pro2 real-time system was used (1 GHz ADSP T12) to supply the voltage (16-bit digital-to-analog convertor card) and to record the QPC detector signal (18-bit analog-to-digital convertor card) for the statistical analysis. The a.c. signals were also generated by the ADwin system. The input and output sampling rates were $\Gamma_S = 400$ kHz.

To minimize the crosstalk with the drive, the detector was kept at a constant working point by periodically adjusting the QPC gate voltage $V_{qpc}(t)$.

The detector current $I_{qpc}(t)$ was monitored with a temporal resolution of $\Delta t_s = 2.5$ μs. For significant statistics we always recorded traces for a duration of 10 min, typically extended over 10^5–10^7 driving periods and containing approximately 10^6 tunnelling events.

Extraction of tunnelling rates. Starting from a long detector trace of alternating in and out states the numbers $N_{in}(t_e)$ ($N_{out}(t_e)$) with which an electron has entered (left) the quantum dot within a bin of width Δt_s around $t_e = t \bmod T_f$ and the numbers $N_0(t_e)$ ($N_1(t_e)$) representing how often the quantum dot is empty (occupied) within the same bin are determined. On the basis of these numbers one can estimate the conditional probabilities of a transition to the occupied state within the interval Δt_s as $p(1, t+\Delta t_s|0, t) = N_{in}(t_e)/N_0(t_e)$ and, similarly, of a transition to an empty dot as $p(0, t+\Delta t_s|1, t) = N_{out}(t_e)/N_1(t_e)$. For a sufficiently small bin width Δt_s, the conditional probabilities can be expanded as $p(1, t+\Delta t_s|0) \approx \Gamma_{in}(t)\Delta t_s$ and $(0, t+\Delta t_s|1) \approx \Gamma_{out}(t)\Delta t_s$, yielding for the time-periodically varying rates

$$\begin{aligned}\Gamma_{in}(t) &= \frac{1}{\Delta t_s}\frac{N_{in}(t_e)}{N_0(t_e)}\\ \Gamma_{out}(t) &= \frac{1}{\Delta t_s}\frac{N_{out}(t_e)}{N_1(t_e)}\end{aligned} \tag{4}$$

The dots in Fig. 3a represent the results of equation (4) for bin width $\Delta t_s = T_f/500$. Solid lines are fits based on a Fourier expansion of the logarithm of the rate with at most three higher harmonics. The experimental in and out rates do not cross exactly at $t = 0$, $T_f/2$, …, because the charging state was not perfectly adjusted to the symmetry level μ_S. Also, the experimental rates differ slightly in their form. This has two main causes. First, the two tunnelling processes are differently affected due the twofold spin degeneracy of the first charging state[29,30], which slightly shifts the symmetry level $\mu_S = \mu_F + k_B T/\sqrt{2}$ above the Fermi level μ_F. Second, the a.c. drive also modulates the size of the tunnelling barriers.

Generally, the in and out rates exhibit a non-trivial dependence on the driving frequency f. Because, in the present case, the driving frequency f is much smaller than any electronic or phononic timescale relevant for the tunnelling process of an electron, the rates depend adiabatically on the frequency f, that is $\Gamma_{in/out}(t, f) = \Gamma_{in/out}(tf/\bar{f}, \bar{f})$, where $\bar{f}$ is a reference frequency, which we chose as $\bar{f} = 800$ Hz.

Counting statistics. For the two-state Markov process with periodically time-dependent rates $\Gamma_{in}(t)$ and $\Gamma_{out}(t)$, the probabilities $p_\alpha(n;t, s)$ to find the quantum dot at time s in the empty or the occupied state $\alpha = 0, 1$, respectively, and to observe n transitions until the time $t > s$ can be calculated as the solution of a hierarchy of first-order differential equations with respect to time t (refs. [13,14]). This hierarchy can be solved successively starting at $n = 0$. Choosing in $p_\alpha(n;t, s)$ the later time as $t = T_f + s$ with $0 \le s < T_f$ one obtains the counting statistics $P(n;s) = p_0(n, T_f + s, s) + p_1(n, T_f + s, s)$ for the number of transitions within a period, which still depend on the initial phase $2\pi s/T_f$ at which the counting window begins. For a comparison with the experimental, phase-averaged results the mean over this phase is performed, yielding the averaged counting statistics $P(n) = \int_0^{T_f} \mathrm{d}s P(n;s)/T_f$, from which the moments of n and the Fano factor can be determined. The theoretical results for the first moment of the number of transitions and the Fano factor are in good agreement with the respective direct experimental outcomes, as can be seen from Figs. 2 and 4. The average number of transitions per period at the minimum is only slightly larger than two, in accordance with the matching condition of the driving frequency with the average Rice frequency defined as the rate of transition events into the occupied state[12,13].

Residence time p.d.f. The residence time p.d.f. $\rho_1(\tau)$ can be obtained in terms of the conditional p.d.f. $\rho(\tau|s) = \Gamma_{out}(\tau+s)P_1(\tau+s|s)$ to find the quantum dot occupied without interruption during the time span $(s, s+\tau)$, where $P_1(\tau+s \mid s) = \exp\left\{-\int_s^{\tau+s}\mathrm{d}t\Gamma_{out}(t)\right\}$ denotes the probability for a quantum dot being permanently occupied from s to $\tau+s$. To obtain the residence time p.d.f. the conditional p.d.f. $\rho_1(\tau|s)$ must be averaged with respect to the time s at which an electron occupies the quantum dot. These events occur according to the p.d.f. $\rho_{in}(s) = \Gamma_{in}(s)p_0(s)/\int_0^{T_f}\Gamma_{in}(s)p_0(s)$. Because we disregard initial transients, the probability $p_0(s)$ to find the quantum dot unoccupied at time s is determined as the asymptotic, and hence periodic, solution of the master equation $\dot{p}_0(t) = -[\Gamma_{in}(t) + \Gamma_{out}(t)]p_0(t) + \Gamma_{out}(t)$. This yields, for the residence time, the result p.d.f.[14]

$$\rho_1(\tau) = \frac{\int_0^{T_f}\mathrm{d}s\Gamma_{out}(\tau+s \mid s)P_1(\tau+s \mid s)\Gamma_{in}(s)p_0(s)}{\int_0^{T_f}\mathrm{d}s\Gamma_{in}(s)p_0(s)} \tag{5}$$

Because the two tunnelling rates $\Gamma_{in/out}(t)$ differ in phase but only little in form, the residence time probability density $\rho_0(\tau)$ for the unoccupied (intervals between 'out' and 'in' events) quantum dot is almost identical to that of the occupied quantum dot.

Data availability

The data that support the plots within this paper and other findings of this study are available from the corresponding author upon request.

References

29. Bonet, E., Deshmukh, M. M. & Ralph, D. C. Solving rate equations for electron tunneling via discrete quantum states. *Phys. Rev. B* **65**, 045317 (2002).
30. Hofmann, A. et al. Measuring the degeneracy of discrete energy levels using a GaAs/AlGaAs quantum dot. *Phys. Rev. Lett.* **117**, 206803 (2017).